A Physics-Based Device Model of Transient Neutron Damage in Bipolar Junction Transistors

Eric R. Keiter, *Member, IEEE*, Thomas V. Russo, Charles E. Hembree, and Kenneth E. Kambour

***Abstract*—For the purpose of simulating the effects of neutron radiation damage on bipolar circuit performance, a bipolar junction transistor (BJT) compact model incorporating displacement damage effects and rapid annealing has been developed. A physics-based approach is used to model displacement damage effects, and this modeling approach is implemented as an augmentation to the Gummel-Poon BJT model. The model is presented and implemented in the Xyce circuit simulator, and is shown to agree well with experiments and TCAD simulation, and is shown to be superior to a previous compact modeling approach.**

***Index Terms*—Annealing, bipolar junction transistor (BJT), circuit modeling, displacement damage, neutron radiation effects.**

I. Introduction

TRANSIENT simulation of high fluence pulse-neutron-irradiated circuits containing silicon (Si) devices is difficult for a number of reasons. A myriad of defects is introduced in bulk Si, which subsequently anneal following neutron exposure. These defects can change device band structure and introduce new energy levels in the bandgap. On an atomic level, there are a prohibitive number of mechanisms present, rendering model development very difficult. There has been a limited amount of previous work in this area [1], although defect physics play an important role in related radiation effects of interest, such as total ionizing dose (TID) [2]. However, models developed for TID are generally not applicable to the high fluence levels typical of a fast-burst reactor.

Circuit simulation tools, such as SPICE [3], typically rely on compact models for individual electrical components, such as transistors and diodes. Compact models consist of a handful of differential and/or algebraic equations. The detailed TCAD simulation of a single irradiated transistor is a very challenging problem [4]–[6], so distilling all relevant physics into a compact model is even more difficult. As a result, compact modeling of neutron effects has been previously limited to empirical approaches [1], [7], which require a relatively high degree of calibration and are mostly applicable to longer-term postanneal behavior as well as other limitations.

Manuscript received July 16, 2010; revised September 04, 2010; accepted September 27, 2010. Date of current version December 15, 2010.

Sandia National Laboratories is a multi-program laboratory managed and operated by Sandia Corporation, a wholly owned subsidiary of Lockheed Martin Corporation, for the U.S. Department of Energys National Nuclear Security Administration under Contract DE-AC04-94AL85000.

The authors are with Sandia National Laboratories, Albuquerque, NM 87185 USA (e-mail: erkeite@sandia.gov).

Color versions of one or more of the figures in this paper are available online at http://ieeexplore.ieee.org.

Digital Object Identifier 10.1109/TNS.2010.2086483

The purpose of this paper has been to develop a predictive, physics-based compact model (PBM) of Si bipolar junction transistors (BJT), which includes transient neutron effects during the early time period (out to 1 s) following neutron exposure. This model is being developed in the Xyce [8] parallel circuit simulator, a production simulator under development within Sandia National Laboratories (SNL). The approach taken for this model is somewhat nontraditional, in that the model is not truly "compact," requiring several hundred equations. However, it is substantially more efficient than equivalent TCAD calculations, and represents a substantial reduction in computational cost.

This paper is organized as follows. In Section II, a brief description of neutron effects in Si devices is given as well as a description of previous neutron compact models. In Section IV, the new model is described in detail. In Sections VII and VIII, the results from the model are presented, compared with experimental data and other modeling approaches. Section IX contains the final summary of this paper.

II. Background

A. Regimes of BJT Behavior

BJTs are generally considered to have four regimes of behavior [9]. There are two PN junctions in a BJT: 1) the base-emitter (BE) junction, and 2) the collector-base (BC) junction. Each can be either forward or reverse biased. The four regions of operation correspond to combinations of junction bias: forward active, inverted active, saturation, and cutoff.

In general, neutron damage will have the greatest impact in junctions that are forward biased, as minority carrier density will be relatively high in forward bias. For the work presented here, the focus has been modeling the forward-active mode, in which the base emitter is forward biased, and the base collector is reverse biased. In principle, the model can be applied to saturation and reverse active modes as well, if adequate carrier models can be developed for the base collector. For the applications of interest to this paper, low-power and leakage are not of primary concern, so leakage effects that may become significant in cutoff mode are not considered.

B. Effect of Neutrons

Incident neutrons damage a semiconductor lattice by creating crystalline defects, such as vacancies, divacancies, and interstitials. These defects reduce carrier lifetimes by adding energy states in the bandgap, which act as recombination centers in the material. As such, any device characteristic that is dependent upon carrier lifetime is affected by neutron damage. This has the potential to affect many aspects of device behavior [7], [10].

U.S. Government work not protected by U.S. copyright.

Deng *et al.* [1] and Hajghassem *et al.* [10] identified several potential impacts on device behavior, including saturation (intercept) current, high-injection knee current, terminal resistances, and depletion/diffusion capacitances.

For the systems of interest for this paper, the most dominant effect of neutron damage is the reduction of transistor gain, the ratio of collector current to base current. As such, this has been the focus of the modeling effort, although it should be noted that the modeling approach presented could be used to address other effects as well.

III. Previous Modeling Approaches

There have been a handful of neutron-induced displacement damage compact models published for BJTs. Due to the complexity of the problem, previous approaches have all relied upon empirical information. Detailed, physics-based TCAD simulation treatments have recently been published [4]–[6], but these treatments are computationally expensive and have not previously been applied to compact modeling.

Gregory *et al.* [11] presented a method for predicting transistor annealing factors, based on a nomograph derived from experimental data.

The annealing factor is defined as

$$AF(t) = \frac{\beta^{-1}(t) - \beta^{-1}(0)}{\beta^{-1}(\infty) - \beta^{-1}(0)} \tag{1}$$

where $\beta = I_C/I_B$ is the forward emitter gain of the device, which is the ratio of collector current I_C and the base current I_B. In (1), $\beta(0)$ is the pre-neutron-exposure gain, $\beta(\infty)$ is stable post-neutron-exposure gain, and $\beta(t)$ is the time-dependent gain. While this approach was not implemented in a simulator at the time, many of the ideas contained in this paper were used in subsequent compact models.

In a related work, a significant observation was made by Gregory *et al.* [12] on the dependence of annealing rates on injection level and temperature. McMurray and Messenger [13] extended this idea to tie this dependence on electron density in the space-charge region. Wrobel [14] also exploited this idea, presenting the following calibrated equation for the annealing factor

$$\mathrm{AF} = 1.0 + 230\left[n_i \int_0^{\tau+t} e^{qV_{be}/(2kT)} \mathrm{d}t\right]^{-0.2}. \tag{2}$$

One consequence of (2) is that the shape of a post-neutron exposure annealing curve is strongly dependent upon applied bias. While (2) is specifically for the base-emitter junction of a PNP device, it could be adapted to other junctions and/or doping types. This early work highlights the need for any compact model of neutron effects to include a strong bias dependence.

A recent compact model of neutron effects was published by Deng *et al.* [1], which for the purposes of discussion will be referred to as the "Rensselaer Polytechnic Institute (RPI) model." It will be used for comparison in Section VII. The RPI neutron model is built around the Gummel-Poon BJT model, with a nonlinear current source connected across the base and emitter.

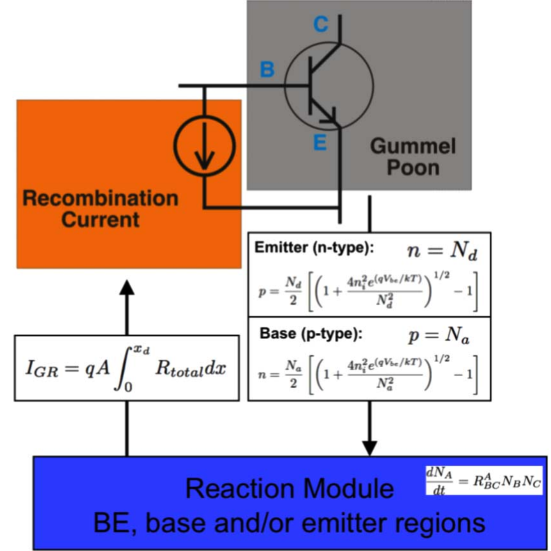

Fig. 1. Neutron model flowchart. In this example, the "core" transistor model is a Gummel-Poon (level $= 1$) BJT, but other transistor models can be used at the discretion of the user.

Functionally, the current source is modeled as a nonlinear function of the collector current.

A limitation of the RPI model is that it has a single time constant to be used in an exponential time dependence of the anneal, as given by [1, (12) and (13)]. As a result, the model cannot be calibrated to more complex annealing curves, and the model is of limited value for cases in which the precise anneal curve shape is important. In addition, injection-level dependence, given by [1, (14) and (15)] is empirical, and difficult to expand for bias states other than forward-active.

IV. Physics-Based Neutron Model Description

In order to provide a predictive capability, a new physics-based model (PBM) of neutron effects in silicon BJTs has been developed. The new model consists of several components, which are illustrated by the flowchart in Fig. 1. This includes a localized reaction model, a carrier model, and an integration term, as well as a normal environment transistor model. For this work, the normal environment model used is the Gummel-Poon BJT model, but other models can be used.

A. Model Assumptions

The use of a global reaction module is based on several assumptions, which are partially based on observations from device (TCAD) simulation. The assumptions include:

- neutron displacement-damage induces a spatially uniform distribution of Frenkel pairs;
- neutron damage-induced recombination is localized to relatively small volumes surrounding forward-biased depletion regions; this assumption is also made in compact models to approximate the Shockley–Read–Hall (SRH) recombination current;[9].
- the primary effect of bias on neutron effects is in the magnitude of the minority carrier densities;
- defect evolution is dominated by reactions and not transport;

- carrier densities are primarily a function of local electrostatic potential and not significantly dependent on recombination;
- defect time scales differ from carrier time scales, allowing for quasistatic approximations of carrier densities.

Some of these assumptions hold more consistently than others. The first assumption—that Frenkel pairs are spatially uniform—is generally not true, as defects tend to form clusters [5]. Accounting for clustering in a physics-based model is computationally prohibitive for a compact model, so it is not included in our model and is only addressed by calibration.

The second assumption holds very well for certain bias states, including the forward-active mode. However, as will be discussed in Sections IV-D and E, there are bias states for which this assumption tends to break, particularly in the base-collector region at high injection. To account for these issues, modifications to the analytic carrier model will be necessary and the subject of future work. For this work, the priority is forward-active mode.

Fortunately, the rest of the assumptions hold for a wide variety of conditions. This is crucial to the conceptual design of the model, in which the carriers are treated separately, and in a numerically different manner than the rest of the defect chemistry. Handling electrons and holes separately allows the model to be less computationally stiff, and less dependent on the transport time scale of carriers. By exploiting this time-scale separation, the model is much more efficient than TCAD-based models.

B. Reaction Module

Neutrons affect BJT performance primarily by creating crystalline defects, which can dramatically increase the carrier recombination rate. Our new neutron model is primarily based on a detailed "reaction module," which solves a set of coupled ordinary differential equations with respect to time, for the full system of defect reactions. The reactants of the model are the set of defect species found in neutron-irradiated silicon: vacancies, divacancies and interstitials of silicon as well as the dopants, which are often boron and phosphorus. For the purposes of the discussion, the defect species, referred to in the rest of this section , are specific to Sin doped with boron and phosphorus, but the same general approach could be used for other materials and dopants.

Carrier emission and capture reactions are included in the model, but are not completely self-consistent, as the electron and hole densities are computed using analytical functions of junction bias. (The details of this analytic calculation are explained in Sections IV-C–E.) As the carrier densities are computed in this manner, they are used as inputs to the reaction module and, thus, the reaction module does not directly compute carrier density.

The relationship between the carrier model and reaction module is illustrated in Fig. 1. The calculated emission and capture rates are used to produce a dynamic recombination current, which is applied in parallel to the Gummel-Poon, also depicted in Fig. 1.

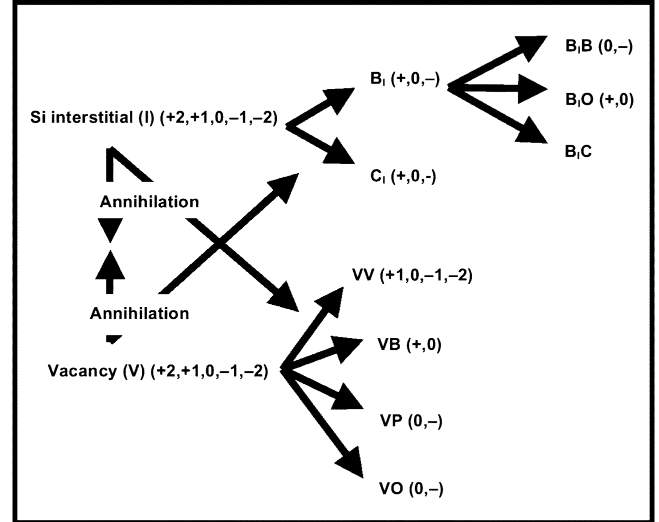

Fig. 2. Defect reaction diagram. Based on the reaction set in Myers [4], [5]. (b) = boron, Si = silicon, V = vacancy, VV = divacancy, O = oxygen. (c)=carbon. The numbers and symbols in parentheses refer to charge states. This reaction set is a subset of all possible defect reactions and species for bulk Si. It was reduced to only include reactions within the first second post-exposure, which is the focus of our paper.

Most of the equations of the global model are of the form

$$\frac{dN_A(t)}{\mathrm{dt}} = k^A_{BC} N_B(t) N_C(t) \tag{3}$$

or

$$\frac{dN_A(t)}{\mathrm{dt}} = k^A_{BC} N_B(t) N_C(t) + S_A(t) \tag{4}$$

where N_A is the concentration of a defect that is produced by a reaction between species N_B and N_C, S_A is a time-dependent source rate, and k^A_{BC} is the reaction rate. S_A is applied to Frenkel pair species (a neutral silicon interstitial and a neutral silicon vacancy) produced by the neutron pulse. The defect transport is excluded, but the module is applied at points on a numerical grid, which extends through the regions of interest. Generally, the region of interest will be the area surrounding the depletion region of a forward-biased junction, and the grid will be the same grid as used by the carrier model described in Section IV-C. Note that in contrast to TCAD, this grid does not cover the entire spatial extent of the device, just the isolated regions of interest. This is one reason why our approach is significantly less computationally expensive than TCAD.

As noted, the model provides carrier emission and capture rates and lifetimes, which are used to produce a recombination current to be applied in parallel to the Gummel-Poon.

A typical reaction network for neutron-induced defects in Si is depicted in Fig. 2. The specific reaction set can be specified from an input file. To date, the reaction networks have been specific to Si devices, but other materials, such as gallium arsenide, could be handled in theory. The reaction network for Si used in this paper has been presented in detail in [4] and [5], so it will not be reprinted here. The reaction set given in [4] and [5] is a subset of all possible defect species and reactions for neutron-irradiated Si. Low-impact species and reactions (particu-

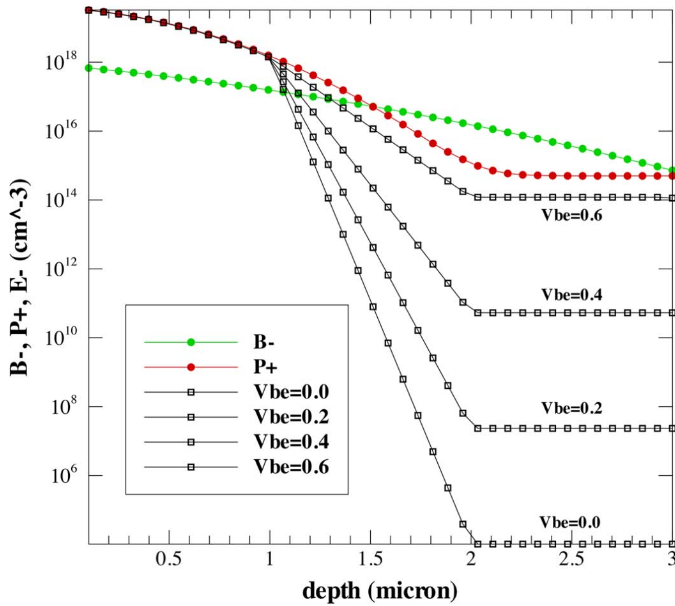

Fig. 3. Electron calculation result. This is from the base-emitter region of a 2N2222. The dopants are boron and phosphorus and their profiles were determined from spreading resistance measurements and SIMS data. On the emitter N-side of the junction, the electron density is pinned to the majority dopant, phosphorus. On the base P-side of the junction, the electrons are the minority carrier and, thus, are computed based on the formula given by (5).

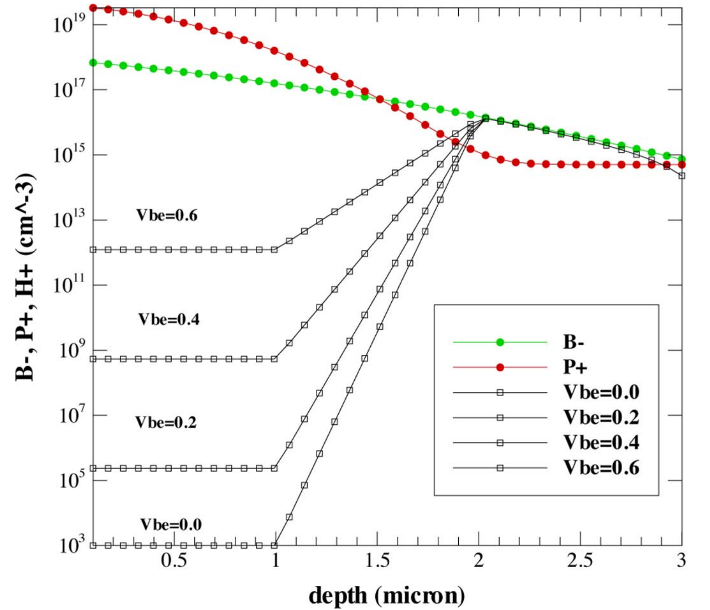

Fig. 4. Hole calculation result. This is from the base-emitter region of a 2N2222. The dopants are boron and phosphorus and their profiles were determined from spreading resistance measurements and SIMS data. On the base P-side of the junction, the hole density is pinned to the majority dopant, boron. On the emitter N-side of the junction, the holes are the minority carrier and,thus,are computed based on the formula given by (6).

larly, reactions with longer timescales) have been excluded for computational efficiency.

C. Carrier Model

The reaction module needs electron and hole densities, as they are reactants in the emission and capture reactions. Typical compact models, such as the Gummel-Poon, do not calculate carrier densities directly, but instead only use currents and voltages as model variables. To approximate the carrier densities needed by the reaction model, a set of analytic expressions and approximations are used, which are computed throughout the integration volume to determine densities as a function of spatial location. It has been observed that the electron and hole densities in the irradiated case will be similar to those of the normal scenario, even during the radiation pulse. As such, one can approximate electron and hole densities with standard analytic expressions, derived for unirradiated devices.

The electron and hole densities at various locations in the device are determined by a combination of approximations. These are illustrated in Figs. 3 and 4.

To obtain the electron and hole densities, the emitter or base region, one assumes that the majority carrier density will be approximately equal to the net doping density. The minority carrier density can be determined from bias-dependent analytic expressions. Thus, the minority carrier density in an p-type region (the base of an NPN transistor), at the junction edge will be ([15, p. 331],

$$n = \frac{N_a}{2}\left[\left(1+\frac{4n_i^2 e^{(qV_{be}/kT)}}{N_a^2}\right)^{1/2} - 1\right]. \tag{5}$$

Equation (5) is derived for the high-injection case, but defaults to a simpler expression for low njection. A similar expression for the minority carrier density in an n-type region (the emitter of an NPN transistor), at the junction edge, will be

$$p = \frac{N_d}{2}\left[\left(1+\frac{4n_i^2 e^{(qV_{be}/kT)}}{N_d^2}\right)^{1/2} - 1\right]. \tag{6}$$

In the middle of the junction, both electron and hole densities are approximated by a logarithmic interpolation between the values of each carrier at the junction edges. This can be observed in Fig. 3 and 4. In the current implementation of the model, the location of the depletion region edge is fixed and not dependent upon bias. In reality, the depletion region width is weakly dependent on applied bias, on the order of $V^{1/r}$, where r is between 2 and 3. However, the depletion width dependence is overshadowed by the much stronger exponential dependence exhibited by the minority carrier densities.

D. Saturation Carrier Model

Section IV-C described the carrier equations for the base-emitter junction region, assuming this function is operating under forward bias. If the transistor is in forward active mode, then only this junction region needs to be included in the model and treatment in Section IV-C is adequate. However, for other bias states, the base collector may need to be considered. In particular, for devices operating in saturation, in which both junctions are operating under forward bias, the neutron model needs to include carrier models (and defect physics modules) for both junctions.

For a device in saturation, applying the model described in Section IV-C without modification to both junctions is sufficient. However, for devices that have the potential to change state, a different model is required for the base-collector junction.

E. Carrier Model for State Transitions

For devices that may switch states from saturation to forward-active, a more rigorous carrier modeling approach is required. For the base-emitter region, the assumptions of Section IV-A hold. However, for the base collector, many of these assumptions break, particularly when the base collector is in reverse bias under high injection. This issue will be the subject of a future publication.

F. Calculation of Recombination Current

The generation-recombination current is determined by using the calculated emission and capture rates for electrons and holes, and integrating over the area of interest

$$I = qA\int_{x_p}^{x_n} R_{\text{total}}dx \tag{7}$$

$$R_{\text{total}} = \sum_{m=1}^{N_{\text{cap}}} R_m^n - \sum_{m=1}^{N_{\text{emit}}} R_m^n + \sum_{m=1}^{N_{\text{cap}}} R_m^p - \sum_{m=1}^{N_{\text{emit}}} R_m^p \tag{8}$$

where A is the cross-sectional area of the device near the depletion region. x_p and x_n define the integration volume boundaries on the p and n side of the junction region, respectively. The integrand in (7) contains the calculated emission and capture rates for electrons and holes from the reaction model, as described by (8). R_{total} is the total rate, R_m^n, R_m^p are recombination rates for electrons and holes and N_{cap}, N_{emit} are the number of capture and emission reactions.

V. Model Calibration

As is clear from the aforementioned discussion, there are many different inputs to the neutron model, including defect reaction rates, transport coefficients, doping profiles, and depletion region width. Addressing all of these inputs directly, as part of a calibration process is not practical. Fortunately, the majority of the input parameters come from experimental data of unirradiated devices, TCAD device simulations, construction analysis, or a combination of these. The reaction network rates and physical parameters are not part of the calibration and are held fixed. The two major parts of the model—the carrier model and the reaction model—are calibrated separately.

A. Calibrating the Carrier Model

Figs. 5 and 6 show the results of an example carrier model calibration for an MMBT2907 PNP transistor (the hole calibration looks similar, but is excluded for brevity). The purpose of this calibration is to obtain the compact carrier model to accurately represent the dependence of minority carrier density on applied bias. Since it is not possible to determine carrier profiles as a function of bias experimentally, this calibration must be performed against TCAD calculations. Since the carrier model expressions are independent of the recombination rate

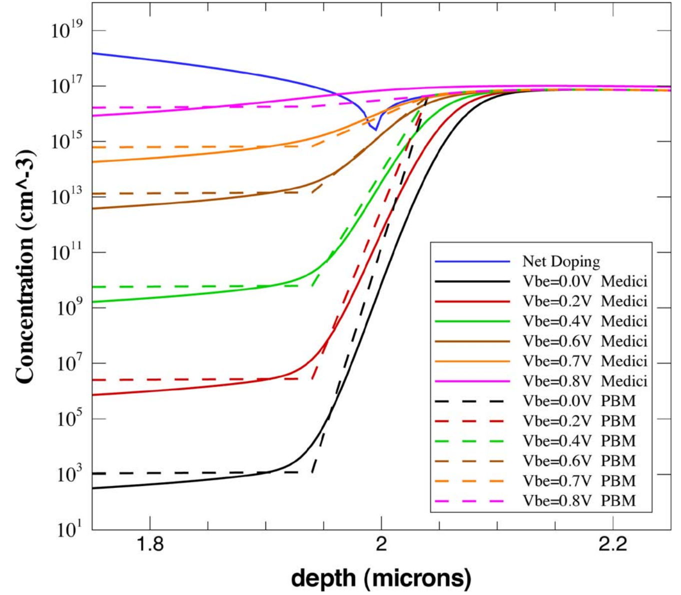

Fig. 5. Calculated compact physics-based model (dashed lines) and TCAD [16] (solid lines) electron densities for an MMBT2907 PNP device for the region surrounding the base-emitter junction, for a range of applied bias.

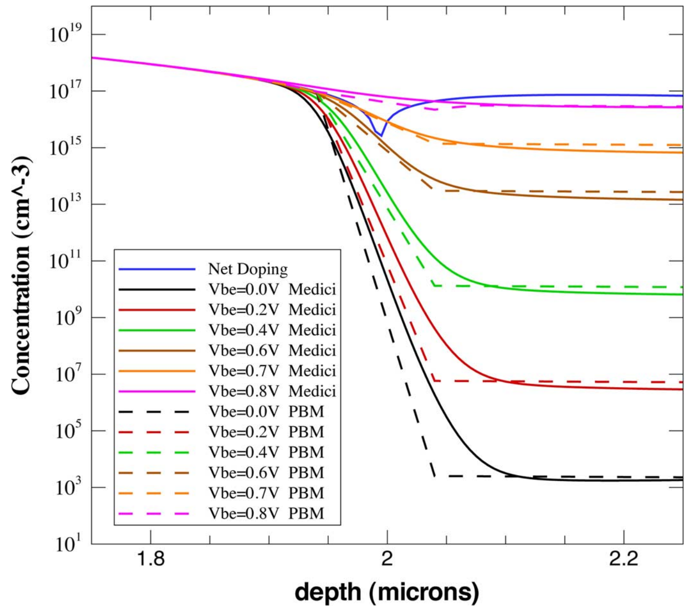

Fig. 6. Calculated compact physics-based model (dashed lines) and TCAD [16] (solid lines) hole densities for an MMBT2907 PNP device for the region surrounding the base-emitter junction for a range of applied bias.

(and, thus, independent of the defect reactions), one can calibrate to a TCAD calculation of an unirradiated device. Thus, a commercial simulator, such as Taurus Medici [16], is adequate for this task.

Note that in Figs. 5 and 6, the compact model result and the TCAD result match well for the overall magnitude of carrier density at a wide range of bias. The discrepancy between TCAD and the compact model primarily comes from the width of the depletion region which, in this version of the compact model, is held to a fixed user-specified value. As noted in Section IV-C,

there should be a small dependence on applied bias, and this can be seen in the TCAD results in both plots. This will be addressed in a future version of the compact model. However, for neutron effects simulation, this should have a relatively small impact on the annealing curve calculation,since the majority of recombination current will be produced inside the depletion region. In addition, as noted earlier, the minority carrier density has a much stronger dependence on bias.

B. Calibrating the Reaction Model

The reaction model itself, which consists of a set of defect species and reactions, is calibrated within the context of TCAD calculation. For the purposes of this compact model, the various defects and reactions as well as the rates and related physical constants are held fixed. As such, we do not consider anything in the reaction module to be a calibration parameter.

C. Calibrating the Recombination Calculation

Although the constants used by reactions themselves are not considered for calibration, the integration volume—which is set by A and x_{dam} from (7)—is a calibrated quantity. These two parameters represent the main empiricism of the model, as neutron damage is actually created everywhere in the device, and not just in an isolated region. However, due to clustering, this damage is not really uniform, and the majority of recombination current will be produced in regions where both carrier densities are relatively high. Thus, if one looks at Figs. 5 and 6, the majority of recombination current will originate near the intersection of the electron and hole density, and the region of interest will be relatively small, within the depletion region. However, since the model is unable to account for defect clustering and, thus, assumes a uniform distribution of defects within the integration volume, the precise size of the volume must be empirically fit.

These two parameters (A and x_{dam}) can theoretically be fitted using either experimental or TCAD data for an irradiated device. To calibrate against TCAD, the TCAD simulator would need to contain a full defect transport/reaction capability, in addition to the standard drift-diffusion equations for electrons and holes, so typical commercial TCAD simulators, such as Taurus Medici, would not be suitable. However, this type of capability is contained in the simulators described in [5] and [17], so this type of calibration is theoretically possible for cases in which experimental data are lacking. For this example, the reaction module is calibrated against experimental data taken from the Annular Core Research Reactor (ACRR) at SNL.

The cross-sectional area parameter A nominally corresponds to a physical quantity, the measured cross-sectional area near the depletion region that is perpendicular to the depletion region width. The damage region width x_{dam} is the width of the damaged region around a point x_{cen} near the center of the depletion region and defines the integration volume boundaries $x_n = x_{\mathrm{cen}} + x_{\mathrm{dam}}/2$ and $x_p = x_{\mathrm{cen}} - x_{\mathrm{dam}}/2$ from (7).

Multiple simulations show that A controls the magnitude of inverse gain of the device at a specific time, while not affecting the shape. Inversely, x_{dam} controls the slope of the inverse gain curve for a given A, while being mostly independent of magnitude.

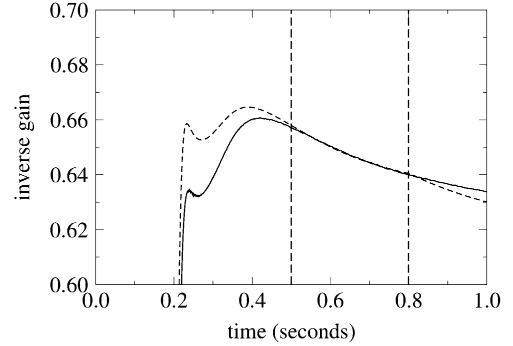

Fig. 7. Fitted simulation for MMBT2907 (dashed curve) and corresponding experimental data (solid curve) for a pulse from the Annular Core Research Reactor (ACRR). The vertical dashed lines represent the time range over which the data were fit.

The calibration process is as follows. The damage region width x_{dam} is initially assumed to be the same as the depletion region width x_d, and A is found by minimizing the difference between the experimentally measured transient inverse gain for the device and the predicted transient inverse gain for a range of time following the radiation pulse. It has been observed that the neutron model overestimates the damage during the peak of the radiation pulse and immediately after, so the time range used for calibration needs to avoid starting too soon after the peak of the pulse.

Once a value for A is found, the value of x_{dam} is fit. In order to better separate the effect of changing x_{dam} from the effect of changing A, x_{dam} is fit to the modified inverse gain, $\beta_{\mathrm{mod}}^{-1}$, which provides a representation of the shape of the anneal curve independent of damage level and emitter current. The expression for $\beta_{\mathrm{mod}}^{-1}$ has been determined empirically and is defined as

$$\beta_{\mathrm{mod}}^{-1}(t) = C_{\mathrm{norm}}^{-1} \frac{I_B(t)}{I_C(t)^{1/3} I_E(t)^{2/3}} \tag{9}$$

$$C_{\mathrm{norm}} = \frac{I_B(t_{\mathrm{norm}})}{I_C(t_{\mathrm{norm}})^{1/3} I_E(t_{\mathrm{norm}})^{2/3}} \tag{10}$$

where C_{norm} is a normalization constant determined at a time several pulsewidths following the pulse peak. I_B, I_C, and I_E are the base, collector, and emitter currents, respectively. The x_{dam} value is determined by minimizing the difference between the simulated $\beta_{\mathrm{mod}}^{-1}(t)$ and experimental $\beta_{\mathrm{mod}}^{-1}(t)$. Using the new value of x_{dam}, the fitting of A is repeated. The process cycles until the values converge.

A final fitting for an MMBT2907 is shown in Fig. 7 along with the experimental data which produced the fit. The change in inverse gain as a function of time for the device as it undergoes a radiation pulse is shown. The radiation pulse peaks at approximately 0.25 s and has measurable neutron fluence out to 0.8 s. This is a typical pulse for a water moderated, moderate fluence reactor, such as the Annular Core Research Reactor (ACRR) at SNL. The fitted values for the two devices of interest are given in Table I.

The model is fit so that the simulation result matches the experimental curve for the time period between the two vertical dashed lines in the plot. The simulated result overpredicts the inverse gain in the early time after the pulse (prior to $t = 0.5$

TABLE I
FITTED VALUES FOR x_d, x_{dam}, AND A, AND VALUES FOR A_{emit}, THE MEASURED EMITTER AREA

Parameter	MMBT2907	2N2222
x_d	$0.10 \times 10^{-4} cm$	$0.13 \times 10^{-4} cm$
x_{dam}	$0.10 \times 10^{-4} cm$	$0.19 \times 10^{-4} cm$
A	$3.52 \times 10^{-4} cm^2$	$1.71 \times 10^{-4} cm^2$
A_{emit}	$4.23 \times 10^{-4} cm^2$	$3.37 \times 10^{-4} cm^2$

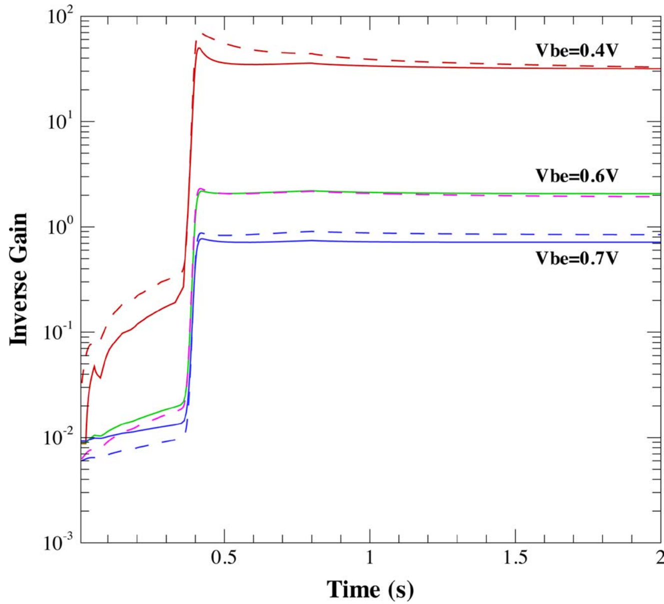

Fig. 8. Xyce simulations for MMBT2907 (dashed curves) and corresponding Charon simulations (solid curves) for a pulse from the Annular Core Research Reactor (ACRR). The label for each curve indicates the emitter-base bias.

s), and under-predicts the data at later times (after $t = 0.8$ s). We believe that the early overprediction is due to inaccuracies in the model at early times, due to a lack of measurable data for quantities, such as interstitial diffusivities. The underprediction at late times is due to the model excluding clustering and defect transport, and is due to the fact that defect reactions that are only significant past times of 1 s were excluded from the reaction model.

VI. Comparison with TCAD

Using the calibration described in Section V, the new physics-based compact model has been compared to the Charon TCAD simulator [17]. Charon is a finite-element semiconductor device simulator which, in addition to carrier drift diffusion equations, includes transport and reaction terms for neutron-induced defects. As compact models are lower-fidelity models than TCAD, comparisons to TCAD are a good test of the assumptions inherent in the compact model.

The model comparison is conducted for two different radiation conditions for a range of applied bias. The first comparison is illustrated in Fig. 8 for a relatively long radiation pulse from ACRR. This is also the condition to which the model was calibrated as is described in the previous section. The second comparison is illustrated in Fig. 9 and is for a radiation pulse from a fast burst reactor (such as the Sandia Pulsed Reactor—SPR). This pulse has relatively high neutron fluence and a full-width half maximum (FWHM) of approximately 100 μs. For this comparison, the same calibration of the compact model was used. In other words, a long-pulse calibration (to ACRR) was used to predict a fast-burst result (SPR).

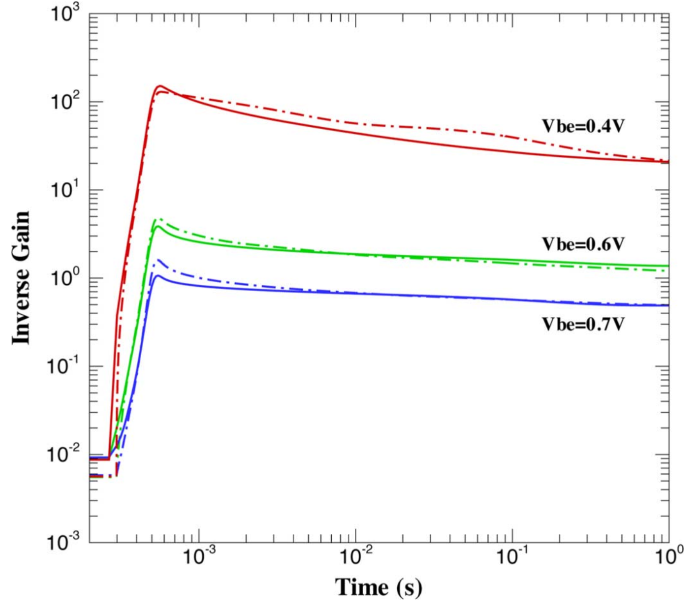

Fig. 9. Xyce simulations for MMBT2907 (dashed curves) and corresponding Charon simulations (solid curves) for a pulse from the Sandia Pulsed Reactor (SPR). The compact model was calibrated to ACRR 0.6 V emiiter-base bias data.

In both cases, the compact model compares well with the TCAD result from Charon. For the ACRR and the SPR result, the model diverges the most for an applied bias of $V_{be} = 0.4$ V. Since the model was calibrated to $V_{be} = 0.6$, this is to be expected. As noted in Section IV-C, the carrier model uses a fixed depletion width, so the farther away the model is from the calibration point, the less accurate the carrier calculation will be.

VII. Compact Model Comparison

Another important comparison is to compare the new model with other compact models. The result of this comparison for the new model is shown in Fig. 10, in which the new compact model is compared against the compact model from [1], referred to as the RPI model. This comparison focuses on dependence on the base-emitter voltage, which is known to have a significant impact on the annealing rate [12]–[14]. In general, increasing forward bias will lead to faster annealing, because defect reaction chemistry is driven in part by the electron and hole densities. The two biases used in the figure are $V_{be} = 0.2$ V and $V_{be} = 0.6$ V. The differences between the models is best illustrated with a shorter radiation pulse which allows the annealing behavior of the inverse gain to be attenuated. For this comparison, a fast burst reactor (SPR) pulse is used in the simulations.

There are several features of interest in Fig. 10. First of all, we found that it was impossible to calibrate the RPI model to match the new physics-based compact model at both values of V_{be}. In addition, the shape of the RPI model annealing curve is constant for both values as well. The RPI model assumes a single time constant, independent upon applied bias. The new

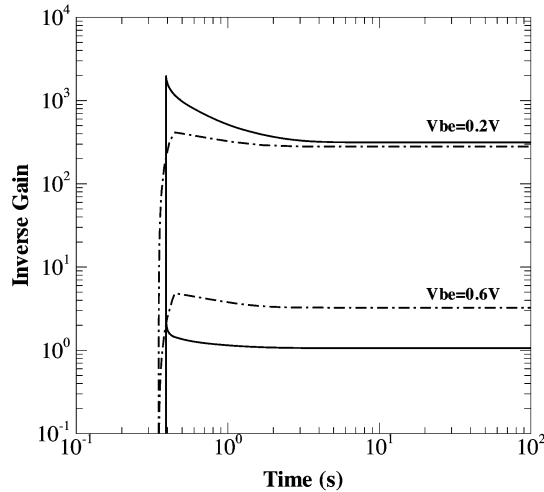

Fig. 10. Neutron compact model comparison. The new physics-based compact model (solid) is compared to the compact model from [1] (dashed). The simulated device is an NPN 2N2222 in forward active mode. For both models, the dashed lines are for $V_{be} = 0.2$ V, and the solid lines are for $V_{be} = 0.6$ V.

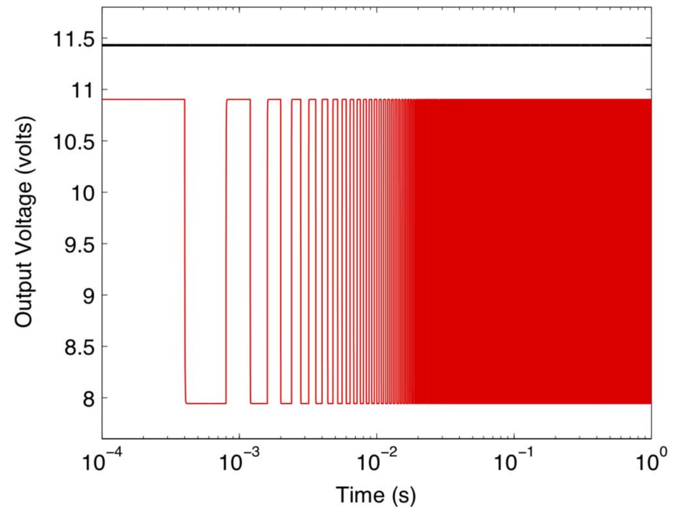

Fig. 12. Circuit output signal, unirradiated case. The right-hand output voltage signal is the gray square wave. The left-hand reference output is the black signal at ~ 11.5 volts.

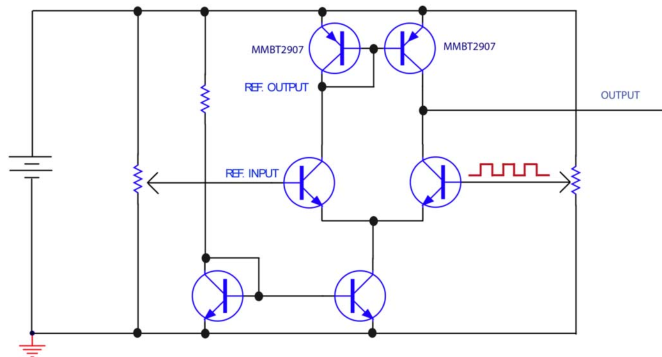

Fig. 11. Neutron model is applied to a differential amplifier circuit.

compact model, in contrast, has a strong bias dependence enforced by the carrier model. As a result, the shape of the new model annealing curve is substantially different for both biases.

VIII. Circuit Applications

The neutron model has been applied to the devices shown in the differential amplifier circuit depicted in Fig. 11. The labeled devices are PNP BJTs whereas the unlabeled devices are NPN BJTs and the model has been calibrated for both polarities of BJTs. In order to account for the effects of ionizing radiation, these devices are also modeled with the photocurrent model presented in [18]. This model is based on a combination of prompt and delay photocurrent terms, in which the delay terms are based on an approximate solution to the ambipolar diffusion equation. The photocurrent models are applied in parallel to the physics-based neutron model. The circuit behavior has been studied at various dose rates and neutron fluences in simulations using a fairly narrow radiation pulse such as that received in a fast burst reactor. As a gain-dependent circuit, this circuit is very sensitive to neutron-induced damage.

In normal environment operation, the output of the circuit returns an amplified version of the input signal shown here in Fig. 11 as a square wave superimposed upon a dc voltage at the right-hand amplifier input. The left-hand amplifier input is a reference voltage. The amplified output signal is slightly offset in voltage from the output reference voltage due to the characteristics of the one-sided long-tailed pair amplifier. The relationship between the reference output and output square-wave signal, prior to radiation, is depicted in Fig. 12.

The asymmetry in the amplifier is exacerbated by neutron radiation damage in the PNP devices. The right-hand output node of the amplifier sees only the current passing through the load PNP device but the left-hand output node of the amplifier sees the current passing through the load PNP device above it and, in addition, the base currents of both load devices. Since these devices are damaged by radiation, their gains decrease and the base currents of each increase. Thus, with radiation exposure, the current through the right-hand output node decreases with respect to the current passing through the left-hand output node and the voltages at the nodes become disparate. This effect increases as radiation exposure increases.

Fig. 13 shows the right-hand output of the amplifier (gray) before, during, and after a radiation pulse of approximately 100 μs duration. The pulse starts at $\sim\ 0.3 \times 10^{-4}$ s and lasts until $\sim 0.3 \times 10^{-3}$ s. The voltage of the output prior to 0.3×10^{-4} s is the normal operational voltage of the amplifier which has a slight offset from the left-hand node (black) reference voltage. During the pulse (0.3×10^{-4} s to 0.3×10^{-3} s), the voltage rises due to the photocurrent induced in the devices by the radiation. After the pulse, the asymmetry of the amplifier is exaggerated by the damage in the devices, and the output voltage drops to the limit imposed by the power supply of the amplifier.

As annealing proceeds, the model predicts that the devices will recover some of the gain, and the amplified input signal begins to appear at the output and gains strength as the annealing in the model allows. In this case, the fluence level of the pulse dictates that only a fraction of the initial gain returns to the devices so the output signal does not recover to pre pulse levels after 1 s or longer times.

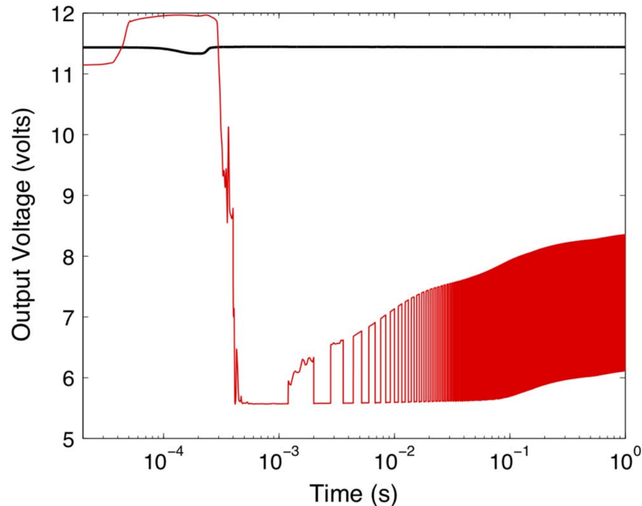

Fig. 13. Right-hand output voltage signal (gray) separates from the left-hand output (black at ~ 11.5 V) as the circuit is exposed to a radiation pulse.

This linear analog circuit exhibits sensitivity to radiation that induces photocurrent and displacement damage. Applying radiation models to circuits of this kind allows exploration of the circuit sensitivities in the proportional shift and catastrophic failure regimes.

IX. Summary and Future Directions

A new approach to neutron-aware compact modeling of BJTs has been described. The new model is based on the evaluation of a detailed reaction model, coupled to a bias-dependent carrier model. The model compares favorably with TCAD simulation data for a range of applied bias.

One of the assumptions of the model, described in Section IV-A, was that the distribution of Frenkel defects in the device is uniform. This is, of course, not a correct assumption, as neutrons will generally create highly localized pockets of damage, sometimes referred to as clusters [5]. This issue is a reason why the model requires a calibrated (rather than measured) cross-sectional area, as well as a damage region smaller than the full device. Future work will focus on mitigating this issue.

As noted in Sections IV-D and E, the carrier profile from the base-collector region can violate some of the assumptions of the new model. Future work will include a new base-collector carrier model, issues such as saturation and the Kirk Effect.

Acknowledgment

The authors would like to thank S. Myers and B. Wampler of SNL for many useful discussions about defect physics in silicon. In addition, the authors would like to thank the Charon development team, including J. Castro and G. Hennigan. Finally, the authors would like to thank the QASPR Program of SNL for financial support.

References

[1] Y. Q. Deng, T. A. Fjeldly, T. Ytterdal, and M. S. Shur, “Spice modeling of neutron displacement damage and annealing effects in bipolar junction transistors,” *IEEE Trans. Nucl. Sci.*, vol. 50, no. 6, pp. 1873–1877, Dec. 2003.

[2] H. Barnaby, I. Esqueda, M. McLain, and X. J. Chen, “Modeling ionizing radiation effects in solid state materials and cmos devices,” *IEEE Trans. Circuits Syst. I, Reg. Papers*, vol. 56, no. 8, pp. 1870–1883, Aug. 2009.

[3] L. W. Nagel, “Spice2: A computer program to simulate semiconductor circuits,” ERL Memo May 1975, (ERL-M5250).

[4] S. Myers, W. Wampler, P. Cooper, and D. King, “Modeling fast-transient defect evolution and carrier recombination in pulse-neutron-irradiated si devices,” *Phys. B: Phys. Condensed Matter*, Jan. 2007.

[5] S. Myers, P. Cooper, and W. Wampler, “Model of defect reactions and the influence of clustering in pulse-neutron-irradiated si,” *J. Appl. Phys.*, Jan. 2008.

[6] H. P. Hjalmarson, R. L. Pease, R. M. Van Ginhoven, P. A. Schultz, and N. A. Modine, “Electrical effects of transient neutron irradiation of silicon devices,” *Nucl. Instrum. Meth. B*, vol. 255, no. 1, pp. 114–119, Jan. 2007.

[7] G. C. Messenger, “A two level model for lifetime reduction process in neutron irradiated silicon and germanium,” *IEEE Trans. Nucl. Sci.*, vol. NS-14, no. 6, pp. 88–102, Dec. 1967.

[8] E. R. Keiter, T. V. Russo, E. L. Rankin, R. L. Schiek, K. R. Santarelli, H. K. Thornquist, D. A. Fixel, T. S. Coffey, and R. P. Pawlowski, Xyce Parallel Electronic Simulator: User’s Guide, Version 5.1 Sandia National Labs, Albuquerque, NM, Tech. Rep. SAND2009-7572, 2009.

[9] M. Shur, *Physics of Semiconductor Devices*. Engelwood Cliffs, NJ: Prentice Hall, 1990.

[10] H. S. Hajghassem, J. R. Yeargan, and W. D. Brown, “Modelling the effects of neutron radiation on the gummel-poon parameters for bipolar npn transistors,” *Microelectron. Reliab.*, vol. 31, no. 5, pp. 969–984, 1991.

[11] B. L. Gregory and H. H. Sander, “Circuit applications of transient annealing,” *IEEE Trans. Nucl. Sci.*, vol. NS-18, no. 6, pp. 250–257, Dec. 1971.

[12] B. Gregory and H. Sander, “Injection dependence of transient annealing in neutron-irradiated silicon devices,” *IEEE Trans. Nucl. Sci.*, vol. NS-14, no. 6, pp. 116–126, Dec. 1967.

[13] L. R. McMurry and G. C. Messenger, “Rapid annealing factor for bipolar silicon devices irradiated by fast neutron pulse,” *IEEE Trans. Nucl. Sci.*, vol. NS-28, no. 6, pp. 4392–4396, Dec. 1981.

[14] T. Wrobel and D. Evans, “Rapid annealing in advanced bipolar microcircuits,” *IEEE Trans. Nucl. Sci.*, vol. 29, no. 6, pp. 1721–1726, Dec. 1982.

[15] R. S. Muller and T. I. Kamins, *Device Electronics for Integrated Circuits*. New York: Wiley, 2003.

[16] TAURUS MEDICI User’s Guide 2006, Synopsys.

[17] G. L. Hennigan, R. J. Hoekstra, J. P. Castro, D. A. Fixel, and J. N. Shadid, “Simulation of neutron radiation damage in silicon semiconductor devices,” Sandia National Laboratories, Albuquerque, NM, Tech. Rep. SAND2007-7157, Oct. 2007.

[18] T. A. Fjeldly, Y. Q. Deng, M. S. Shur, H. P. Hjalmarson, A. Muyshondt, and T. Ytterdal, “Modeling of high-dose-rate transient ionizing radiation effects in bipolar devices,” *IEEE Trans. Nucl. Sci.*, vol. 48, no. 5, pp. 1721–1730, Oct. 2001.